Defects in lysosomal maturation facilitate the activation of innate sensors in systemic lupus erythematosus

Andrew J. Monteith[a,b], SunAh Kang[a], Eric Scott[a], Kai Hillman[a], Zenon Rajfur[c,d], Ken Jacobson[c,e], M. Joseph Costello[c], and Barbara J. Vilen[a,e,1]

[a]Department of Microbiology & Immunology, University of North Carolina, Chapel Hill, NC 27599; [b]Curriculum in Biochemistry & Biophysics, University of North Carolina, Chapel Hill, NC 27599; [c]Department of Cell Biology & Physiology, University of North Carolina, Chapel Hill, NC 27599; [d]Department of Physics, Astronomy, and Applied Computer Science, Institute of Physics, Jagiellonian University, 31-007, Krakow, Poland; and [e]Lineberger Comprehensive Cancer Center, University of North Carolina, Chapel Hill, NC 27599

Edited by Jason G. Cyster, University of California, San Francisco, CA, and approved March 1, 2016 (received for review July 15, 2015)

Defects in clearing apoptotic debris disrupt tissue and immunological homeostasis, leading to autoimmune and inflammatory diseases. Herein, we report that macrophages from lupus-prone MRL/*lpr* mice have impaired lysosomal maturation, resulting in heightened ROS production and attenuated lysosomal acidification. Impaired lysosomal maturation diminishes the ability of lysosomes to degrade apoptotic debris contained within IgG–immune complexes (IgG-ICs) and promotes recycling and the accumulation of nuclear self-antigens at the membrane 72 h after internalization. Diminished degradation of IgG-ICs prolongs the intracellular residency of nucleic acids, leading to the activation of Toll-like receptors. It also promotes phagosomal membrane permeabilization, allowing dsDNA and IgG to leak into the cytosol and activate AIM2 and TRIM21. Collectively, these events promote the accumulation of nuclear antigens and activate innate sensors that drive IFNα production and heightened cell death. These data identify a previously unidentified defect in lysosomal maturation that provides a mechanism for the chronic activation of intracellular innate sensors in systemic lupus erythematosus.

systemic lupus erythematosus | Fc gamma receptors | lysosomal acidification | AIM2 | TRIM21

The disposal of apoptotic debris is initiated by membrane changes that facilitate the binding of IgM antibodies, acute phase proteins (C-reactive protein, CRP), and other serum opsonins to enhance phagocytosis (1, 2). The disposal of apoptotic debris is crucial to immune homeostasis because the accumulation of apoptotic debris (3–5), and the formation of immune complexes (ICs) (6), have long been associated with systemic lupus erythematosus (SLE). Similarly, impaired clearance of apoptotic bodies in mice lacking scavenger receptors and complement proteins induces spontaneous autoimmunity (7, 8). The idea that accumulated apoptotic bodies contribute to SLE is further supported in human studies describing polymorphisms or decreased expression of scavenger receptors, increased expression of FcγRs, or deficiencies in complement (9–14). Despite these findings, it remains unclear whether macrophages (MFs) harbor intrinsic defects that impaired apoptotic cell clearance (15, 16).

Apoptotic debris bound by IgG autoantibodies forms immune complexes [henceforth referred to as IgG–immune complexes (IgG-ICs)] that heighten autoantibody production by chronically stimulating autoreactive B-cell receptors (BCRs) and/or Toll-like receptors (TLRs) upon delivery of nucleic acids to the endosome (17, 18). IgG-ICs also bind FcγRs on myeloid cells stimulating IFNα (19) and BAFF (20) secretion. In addition, activation of cytosolic sensors contributes to the pathology of SLE. Polymorphisms in the sensor that recognizes cytoplasmic IgG (tripartite motif containing 21; TRIM21; ref. 21), and heightened expression of TRIM21 (22) and its regulated genes (22, 23), have been identified in SLE patients. Further, two cytosolic sensors that recognize dsDNA (p202 and absent in melanoma 2; AIM2) have been implicated in type 1 interferon (IFN) production in murine lupus (24, 25). The involvement of other cytosolic sensors, including NLRP3/NLRP1 (26, 27) and STING (28, 29), have been more controversial. Despite the mounting evidence implicating cell debris in the activation of innate sensors, a mechanism explaining how IgG-ICs gain access to the cytosol and chronically activate intracellular receptors/sensors has never been resolved.

Herein, we show that lupus-prone MFs fail to fully mature lysosomes, causing diminished lysosomal acidification and the inability to degrade phagocytosed IgG-ICs. As a result, intact IgG-ICs recycle back to the cell membrane, promoting the accumulation of surface-bound nuclear antigens. The prolonged residency of intracellular IgG-ICs in the phagolysosome leads to membrane permeabilization, allowing dsDNA and IgG to leak into the cytosol and activate AIM2 and TRIM21. Furthermore, accumulation of undegraded nucleic acids inside the phagolysosome leads to the activation of TLR7 and TLR9. The combined activation of these receptors heightens cell death through inflammasome formation and leads to IFNα secretion.

Results

IgG-ICs Accumulate in Multiple Murine Models of Autoimmunity. The accumulation of apoptotic debris has been identified in autoimmune diseases other than SLE, including apoptotic beta cells in diabetes (30), and apoptotic synoviocytes in rheumatoid arthritis (31). We find that MFs from lupus-prone mice (MRL/*lpr* and

Significance

Activation of innate sensors by self-antigen contributes to autoimmunity, although how intracellular sensors are chronically exposed to self-antigen has remained unknown. Here, we identify a previously unidentified defect in which lupus-prone macrophages fail to mature the lysosome, promoting the accumulation of apoptotic debris-containing IgG–immune complexes (IgG-ICs). Interestingly, macrophages from other autoimmune diseases accumulate IgG-ICs, indicating that lysosomal defects may underlie multiple autoimmune diseases. Furthermore, the prolonged intracellular residency chronically activates Toll-like receptors and permeabilizes the phagolysosomal membrane, allowing activation of cytosolic sensors. These findings identify lysosomal maturation as a unique defect in MRL/lpr mice that impacts multiple events known to underlie SLE, including pathogenic cytokine secretion.

Author contributions: A.J.M., S.K., E.S., and B.J.V. designed research; A.J.M., S.K., E.S., K.H., Z.R., and M.J.C. performed research; Z.R., K.A.J., and M.J.C. contributed new reagents/analytic tools; A.J.M., S.K., and E.S. analyzed data; and A.J.M. and B.J.V. wrote the paper.

The authors declare no conflict of interest.

This article is a PNAS Direct Submission.

[1]To whom correspondence should be addressed. Email: barb_vilen@med.unc.edu.

This article contains supporting information online at www.pnas.org/lookup/suppl/doi:10.1073/pnas.1513943113/-/DCSupplemental.

NZM2410) accumulate high levels of FcγR-bound IgG-ICs (Fig. 1) (32). Similarly, SLE patients experiencing active disease accumulate nuclear antigens on peripheral blood mononuclear cells (32). Therefore, we assessed whether the accumulation of IgG-ICs occurs in other autoimmune models by quantifying the levels of surface IgG and nuclear antigen on MFs from murine models of diabetes (NOD) and rheumatoid arthritis (K/BxN). We found that the levels of surface IgG on MFs from NOD and K/BxN mice with active disease were elevated (Fig. 1*C*) and had a punctate staining pattern (Fig. S1) similar to MRL/*lpr* MFs, suggesting aggregated, rather than monomeric, IgG. Surface Sm levels were slightly elevated on NOD MFs, but absent on MFs from K/BxN mice, raising the possibility that in other autoimmune diseases, MFs accumulate aggregated surface IgG that might be part of immune complexes containing disease-specific antigens. Because NOD, MRL/*lpr*, and NZM2410 mice are genetically unrelated, these findings also suggest that multiple distinct genetic defects could lead to the accumulation of immune complexes on the cell surface. Thus, understanding the mechanism underlying the accumulation of IgG-ICs on the surface of MRL/*lpr* MFs could elucidate a fundamental defect in autoimmunity.

Lupus-Prone MFs Phagocytose IgG-ICs but Exhibit Defective Phagolysosome Maturation. In SLE, the accumulation of apoptotic debris has been attributed to heightened cell death, impaired clearance of cell debris, decreased complement, and increased IgG levels (3–5, 33–36). Whether lupus-prone MFs have intrinsic defects contributing to impaired clearance of apoptotic debris is debated because no mechanism has been defined (15, 16). To identify how IgG-ICs accumulate, we formed ICs using anti-nucleosome (PL2.3, IgG2a) bound to apoptotic blebs. The use of apoptotic blebs and autoantibody allows B6 and MRL/*lpr* MFs to internalize physiologically relevant IgG-ICs, and a means to compare phagocytosis, intracellular trafficking, and degradation in real time. Using total internal reflection fluorescence (TIRF) microscopy, we found B6 and MRL/*lpr* MFs had comparable diffusion coefficients before internalization and internalized IgG-ICs at similar rates (Fig. 2 *A* and *B*). Therefore, the accumulation of IgG-ICs on the surface of MRL/*lpr* MFs is not the result of impaired phagocytosis.

Another possible explanation for accumulation of IgG-ICs on MRL/*lpr* MFs is improper trafficking to lysosomes. However, cryo-electron microscopy showed that ∼80% of gold-labeled IgG-ICs reached lysosomal structures in B6 and MRL/*lpr* MFs within 2 h of phagocytosis (Fig. 2 *C* and *D*). Therefore, intracellular trafficking is not impaired.

Impaired lysosomal degradation could promote membrane accumulation of IgG-ICs after internalization and trafficking to lysosomal structures. Lysosomes contain hydrolytic enzymes that degrade cargo entering the cell through multiple receptors, including FcγRs (37). Activation of lysosomal enzymes requires the termination of reactive oxygen species (ROS) production and activation of the vacuolar H^+-ATPase (V-ATPase) to achieve a pH ≤ 5 (38). To determine the pH of maturing phagosomes, we introduced an acidotropic ratiometric dye during phagocytosis of IgG-ICs. In B6 MFs, real-time two-photon microscopy identified vesicular fusion events, resulting in large acidic structures (pH ≤ 4.5) (Fig. 3 *A* and *B*). In MRL/*lpr* MFs, large acidic structures were rarely evident and vesicles failed to sustain a pH below 5.5. To analyze larger numbers of MFs, we used ratiometric flow cytometry to quantify the relative pH of the population. Within 30 min of exposure to IgG-ICs, B6 MFs reduced vesicular pH by 20% then deacidified within 1 h (Fig. 3*C*). Conversely, MRL/*lpr* MFs showed an 8% drop in pH. Concurrent with the inability to fully acidify lysosomes, MRL/*lpr* MFs exhibited heightened and prolonged production of ROS (Fig. S2). These results demonstrate that MRL/*lpr* MFs are functionally impaired in lysosomal acidification, but the impairment is not absolute as seen in lysosomal storage disorders. These findings are consistent with the idea that antigen processing and MHC presentation remain partially intact in lupus-prone mice (39, 40).

The impaired acidification and heightened ROS production suggests that MRL/*lpr* MFs are not properly maturing the phagolysosome, thus preventing the degradation of IgG-ICs. Maturation of the phagolysosome and autophagosome requires membrane stabilization, achieved through the recruitment of lysosome-associated membrane proteins (LAMPs) and light chain 3 (LC3). To assess whether the phagolysosome fully matures, we quantified the levels of LAMP-1 and LC3A to distinguish autophagosomes ($LC3A^+$, $LAMP\text{-}1^-$) and autophagolysosomes ($LC3A^+$, $LAMP\text{-}1^+$) from lysosomes ($LC3A^-$, $LAMP1^+$). Using confocal microscopy, we found that MRL/*lpr* MFs showed a twofold reduction in the association of IgG-ICs with $LC3A^-$, $LAMP\text{-}1^+$ structures (Fig. 3 *D* and *E*). Because IgG-ICs arrive at lysosomal structures (Fig. 2 *C* and *D*), the reduced association of LAMP-1 with vesicles containing IgG-ICs demonstrates that the impaired acidification of the lysosomes is consistent with defective phagolysosome maturation.

Lupus-Prone MFs Recycle IgG-ICs to the Cell Membrane. Damaged membrane proteins traffic to the lysosome for degradation; however, impaired degradation promotes their recycling back to the cell membrane (41, 42). We hypothesized that a similar mechanism might promote recycling and the accumulation of FcγR-bound IgG-ICs because they also are targeted to lysosomal structures following activation (37). To determine whether impaired lysosomal degradation promotes accumulation of surface nuclear antigens, we cocultured MFs with fluorophore-conjugated IgG-ICs and monitored their localization over time. Greater than 75% of the MFs phagocytosed IgG-ICs and both B6 and MRL/*lpr* MFs bound similar levels of IgG-ICs (Fig. 4 *A* and *B*). Bound IgG-ICs were rapidly phagocytosed and evident within vesicular compartments at 24 h. By 72 h, MFs from the MRL/*lpr* mice recycled the IgG-ICs back to the cell membrane, whereas B6 MFs retained them within the cell (Fig. 4 *A* and *B* and Fig. S3). The IgG-ICs appeared to remain intact and bound by FcγRs, because both the antibody and apoptotic debris colocalized on the surface of the cell (Fig. S4), and the levels of surface FcγRI

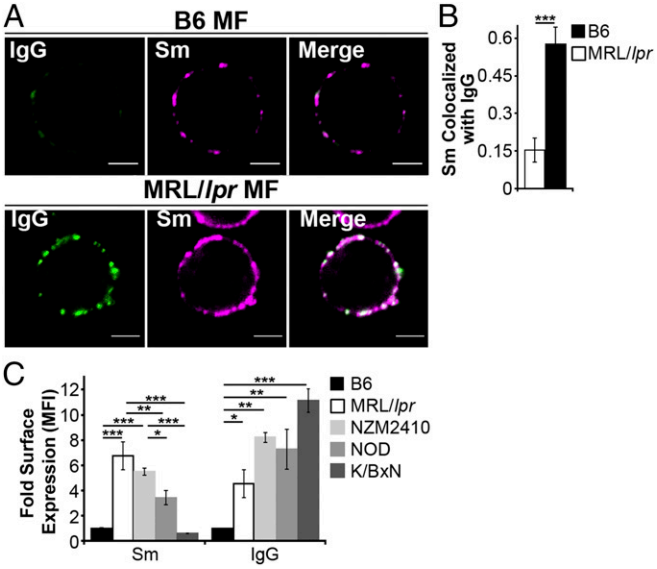

Fig. 1. Autoimmune-prone MFs accumulate IgG-ICs on the cell membrane. (*A* and *B*) $CD11b^+$ cells were purified from spleen and analyzed for surface Sm and IgG by confocal imaging. (Scale bars: 2.5 μm.) Data represent two experiments, two mice, 8–10 cells. A representative image of a MF from the indicated mice (*A*) and quantification of IgG colocalization with Sm for all cells imaged (*B*) is presented. (*C*) Flow cytometry analysis of surface IgG and Sm on splenic MFs ($CD11b^+$, $CD11c^-$) relative to B6 IgG [mean fluorescence intensity (MFI) range = 1.81–7.64] or B6 Sm (MFI range = 1.02–7.55); four experiments, 4–8 mice (B6 ≥ 12 wk, MRL/*lpr* ≥ 12 wk, NZM2410 = 12–22 wk, NOD ≥ 26 wk; blood glucose levels > 500 mg/dL, K/BxN ≥ 13 wk; clinical score = 10). Error bars indicate SEM. Student *t* test or ANOVA, $*P \le 0.05$, $**P \le 0.01$, $***P \le 0.001$.

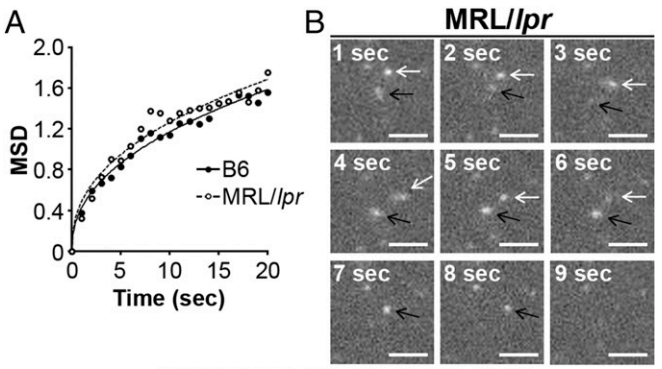

Anomalous Diffusion (MSD = 4Dt$^{\alpha}$)

	Diff Coef. (D)	α	R^2
B6	0.107 ± 0.011	0.438 ± 0.041	0.985
MRL/*lpr*	0.122 ± 0.021	0.415 ± 0.067	0.956

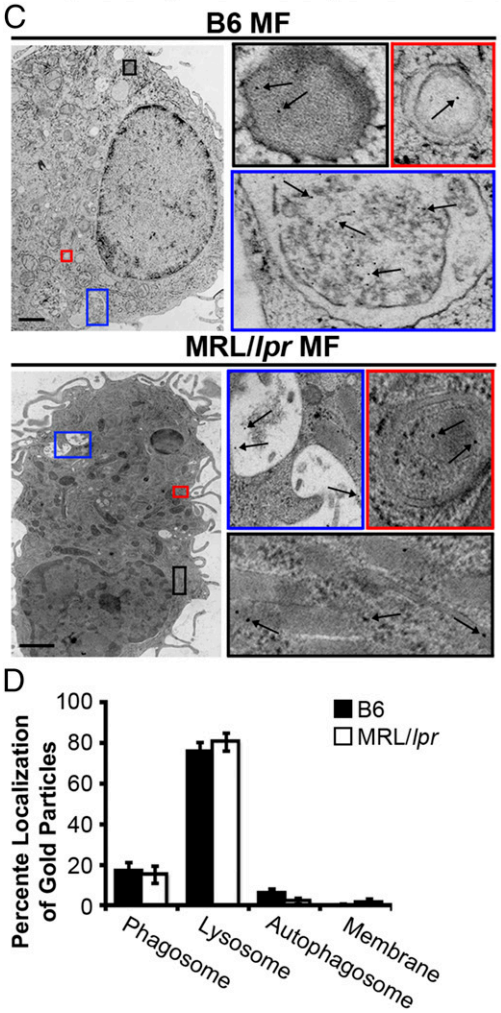

Fig. 2. MRL/*lpr* MFs phagocytose and traffic IgG-ICs to lysosomal structures. (*A* and *B*) Bone marrow-derived macrophages (BMMFs) were cultured with Alexa488-labeled IgG-ICs and examined over time by TIRF microscopy; four experiments, four mice, cells = 9–12, *n* = 47–48. The mean squared displacement (MSD) was calculated by tracking the displacement of IgG-ICs on the surface of the cell until the IgG-IC left the imaging plane (phagocytosis). (*A*) Each point is the average MSD of 4–7 IgG-ICs from two to four cells in the imaging plane. (*B*) A representative time series of IgG-ICs on the surface of a MRL/*lpr* MF (arrows) is presented. (*C* and *D*) BMMFs were cultured with gold-labeled IgG-ICs for 2 h and examined by cryo-electron microscopy; two experiments, two mice, 12–15 cells. A representative image of a MF from the indicated mice (*C*) and the subcellular localization of IgG-ICs in each cell and quantified for all cells imaged (*D*) is presented. IgG-ICs were found in phagosomes (single membrane, electron light), lysosomes (single membrane, electron dense), autophagosomes (double membrane), and on the cell membrane. Error bars = SEM. Student *t* test, $*P \leq 0.05$, $**P \leq 0.01$, $***P \leq 0.001$. (Scale bars: 1 μm.)

and IgG on MRL/*lpr* MFs increased proportionately (32). Overall, these findings support a model wherein impaired maturation of the lysosome in MRL/*lpr* MFs diminishes degradation of IgG-ICs, inducing their recycling back to the membrane.

The levels of nuclear antigen on MFs from MRL/*lpr* mice lacking FcγRI (FcγRI$^{-/-}$MRL/*lpr*) are decreased 60% compared with cells from FcγRI$^{+/+}$MRL/lpr mice, and they remain disease-free (32), implicating the accumulation of IgG-ICs on FcγRI in SLE. Despite FcγRI$^{-/-}$MRL/*lpr* MFs binding 60% fewer IgG-ICs (Fig. 4 *A* and *B*), they remain impaired in lysosomal acidification and recycle internalized IgG-ICs. Therefore, FcγRI is not the only receptor that recycles IgG-ICs, and loss of FcγRI decreases the amount of IgG-ICs that are internalized.

To assess whether recycling is unique to ICs containing apoptotic debris, we bound anti-LPS (IgG2b) to gentamicin-killed *Escherichia coli* (*E. coli*-ICs). Although MRL/*lpr* MFs phagocytosed fewer *E. coli*-ICs (Fig. 4*C*), 72 h following phagocytosis, the levels of LPS on the cell surface increased threefold compared with those on B6 MFs (Fig. 4*D*). These findings indicate that *E. coli*-ICs also fail to be degraded by MRL/*lpr* MFs. To assess whether all ICs were recycled in MRL/*lpr* MFs, we cultured MFs with ICs formed by binding $TNP_{20}KLH$ to anti-TNP IgG2a (TNP-ICs). Surprisingly, both MRL/*lpr* and B6 MFs phagocytosed and degraded the TNP-ICs (Fig. 4*E*, *Right*), unlike IgG-ICs (Fig. 4*E*, *Left*). These data demonstrate that MRL/*lpr* MFs degrade some IgG-ICs, and that recycling is not unique to ICs containing apoptotic debris.

To assess whether impaired lysosomal acidification is sufficient to induce recycling of IgG-ICs, we inhibited lysosome function in B6 MFs and assessed whether this induced IgG-ICs to recycle. Concanamycin A prevents acidification and degradation of phagocytosed cargo by specifically inhibiting the lysosomal V-ATPase. B6 MFs treated with concanamycin A recycled IgG-ICs at levels similar as MRL/*lpr* MFs (Fig. 4*F*). Thus, diminished lysosomal acidification is sufficient to promote recycling and accumulation of IgG-ICs.

Impaired Lysosomal Maturation Permeabilizes the Phagolysosomal Membrane Allowing dsDNA and IgG To Leak into the Cytosol. Studies of microbial pathogens have shown that some intracellular bacteria prevent phagosomal maturation, resulting in bacterial antigens accessing the cytosol (43, 44). In a similar manner, impaired lysosomal maturation in MRL/*lpr* MFs might allow antigens from IgG-ICs to gain access to the cytosol and activate innate sensors. Therefore, we selected two cytosolic sensors (AIM2 and TRIM21) that recognize different components from IgG-ICs (dsDNA and IgG) to determine whether the inability to mature the lysosome permeabilizes the phagolysosome, allowing antigens to leak into the cytosol. To assess whether nuclear antigens gained access to the cytosol, we stimulated B6 and MRL/*lpr* MFs with IgG-ICs containing fluorescent dsDNA. Immunoprecipitation of AIM2 from B6 and MRL/*lpr* MFs showed equal levels of AIM2 protein (Fig. 5*A*). Despite equal amounts of protein, MRL/*lpr* MFs had a 2.5-fold increase in the amount of dsDNA bound to AIM2 compared with B6 (Fig. 5*B*). In contrast, AIM2 from FcγRI$^{-/-}$MRL/*lpr* MFs bound the same level of dsDNA as B6. These findings suggest that although FcγRI$^{-/-}$MRL/*lpr* MFs recycle IgG-ICs (Fig. 4 *A* and *B*), they leak fewer antigens into the cytosol, possibly as a consequence of decreased internalization of IgG-ICs, or because FcγR-specific signals are necessary to permeabilize the phagolysosome.

AIM2 initiates inflammasome formation by recruiting procaspase-1 through the linker molecule ASC resulting in the cleavage and activation of caspase-1 (24). To assess whether phagocytosis of IgG-ICs by MFs induces inflammasome formation, we quantified active caspase-1, and enumerated cytosolic ASC foci (Fig. 5 *C* and

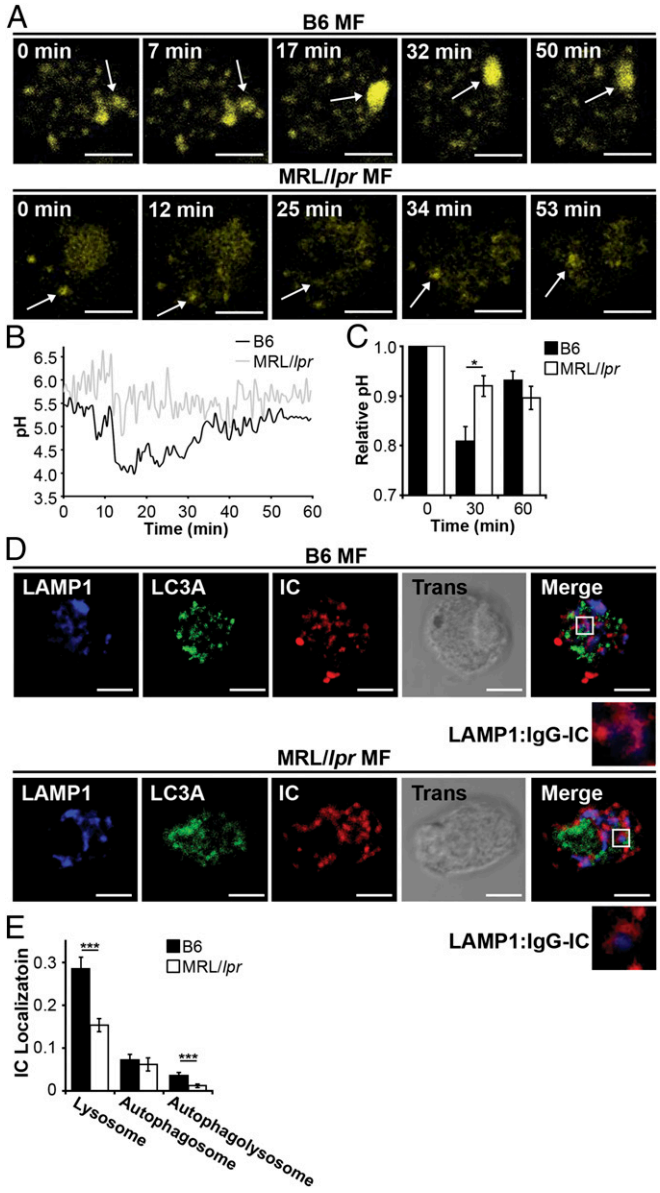

Fig. 3. MRL/*lpr* MFs fail to mature the lysosome. (*A* and *B*) BMMFs were stimulated with IgG-ICs, and the pH of the maturing phagosomes were assessed by ratiometric two-photon microscopy; three experiments, three mice, 10–25 cells. A representative time series of a MF from the indicated mice (*A*) with the quantified pH of a single phagosomal acidification event (arrow) (*B*) is presented. Ratiometric flow cytometry was used to quantify the relative phagosomal pH across the entire population of MFs; six experiments, 6–8 mice (*C*). (*D* and *E*) Colocalization of IgG-ICs with LAMP-1 and/or LC3A was assessed by confocal imaging; three experiments, three mice, 36–39 cells. A representative image of a MF from the indicated mice (*D*) and quantification of IgG-IC colocalization with indicated compartments for all cells imaged (*E*) is presented. Error bars = SEM. Student *t* test, $*P \leq 0.05$, $**P \leq 0.01$, $***P \leq 0.001$. (Scale bars: 5 μm.)

D). In the resting state, the number of MRL/*lpr* MFs containing ASC foci was consistently elevated compared B6 and FcγRI$^{-/-}$MRL/*lpr* MFs, but this difference was not statistically significant. After culturing the MFs for 4 h with IgG-ICs, ∼40% of the MRL/*lpr* MFs exhibited ASC foci compared with 20% in B6 and FcγRI$^{-/-}$ MRL/*lpr* MFs (Fig. 5*D*). This finding was consistent with diminished binding of dsDNA to AIM2 in B6 and FcγRI$^{-/-}$MRL/*lpr* MFs (Fig. 5 *A* and *B*). In MRL/*lpr* MFs, heightened formation of ASC foci coincided with a 4.5-fold increase in active caspase-1 compared with either B6 or FcγRI$^{-/-}$MRL/*lpr* MFs (Fig. 5*E*). Similarly, ex vivo splenic myeloid cells from MRL/*lpr* mice exhibited a twofold increase in active caspase-1 compared with B6 (Fig. 5*F*). Inflammasome formation was the consequence of lysosomal dysfunction because B6 MFs treated with concanamycin A had high levels of ASC foci and caspase-1 activation (Fig. 5 *D* and *E*). Thus, using dsDNA binding to AIM2 as a sentry for phagolysosomal membrane permeabilization, we found that impaired lysosomal degradation of IgG-ICs allows nuclear antigens to leak into the cytosol. These antigens bind AIM2 coincident with the activation of caspase-1 and the formation of inflammasomes. Although it would be ideal to assess the contribution of AIM2 in caspase-1 activation and inflammasome formation in MRL/*lpr* MFs, the heightened ROS production, heterogeneity of the ligands contained in the IgG-ICs, and the number of DNA-binding cytosolic sensors make knockdown of any single sensor unlikely to have an effect.

To corroborate the idea that antigens leak into the cytosol as a consequence of diminished phagolysosomal maturation and membrane permeabization, we assessed whether IgG from exogenous IgG-ICs activated TRIM21, a cytosolic sensor with high affinity for IgG (45). We found that 4 h after coculture with IgG-ICs, MRL/*lpr* MFs showed a twofold increase compared with B6 MFs in fluorophore-tagged IgG bound to TRIM21 (Fig. 6 *A* and *B*). The level of TRIM21-bound IgG in FcγRI$^{-/-}$MRL/*lpr* MFs was not different from B6, indicating that similar to nuclear antigen, diminished internalization of IgG-ICs reduces the amount of IgG reaching the cytosol. Similarly, coculture of MRL/*lpr* MFs with IgG-ICs increased the levels of IgH/IgL bound by TRIM21 (Fig. 6*A*). We do not believe that the heightened levels of IgG bound to TRIM21 are a consequence of the 8.8-fold increase in TRIM21 protein levels in MRL/*lpr* MFs because FcγRI$^{-/-}$MRL/*lpr* MFs also exhibited heightened levels of TRIM21 (Fig. 6 *A* and *C*), and their levels of IgG bound to TRIM21 were not different from B6 (Fig. 6 *A* and *B*). Thus, elevated TRIM21 may contribute to disease pathology, but it alone is insufficient unless diminished lysosomal maturation provides heightened levels of IgG ligand.

TRIM21 is an E3 ligase that possesses two unique functions. First, it inhibits type 1 IFN production by diminishing interferon regulatory factor (IRF) protein levels through ubiquitination and proteasomal degradation. Second, the binding of IgG to TRIM21 stabilizes IRF proteins and activates NF-κB (46, 47), heightening TLR activation and type 1 IFN production. To assess whether TRIM21 was activated, we cocultured B6 and MRL/*lpr* MFs with IgG-ICs and quantified the nuclear translocation of p65 during NF-κB activation. Resting MRL/*lpr* MFs exhibited slightly elevated nuclear p65 levels; however, this difference was not statistically significant. After coculture with IgG-ICs, nuclear translocation of p65 was increased 2.5-fold (Fig. 6 *D* and *E*). Loss of FcγRI in MRL/*lpr* MFs restored nuclear p65 levels to those in B6 MFs. Further, p65 nuclear translocation was the consequence of failed lysosomal acidification because concanamycin A-treated B6 MFs stimulated with IgG-ICs induced a 2.5-fold increase in nuclear p65 (Fig. 6 *D* and *E*). It was possible that NF-κB activation in response to IgG-ICs resulted from the binding of apoptotic debris to intracellular TLRs. To assess this possibility, we cocultured MRL/*lpr* MFs with apoptotic blebs lacking IgG. Like IgG-ICs, apoptotic blebs recycled in MRL/*lpr* MF (Fig. S5) possibly because they are opsonized by CRP and enter cells via FcγRI (48). Despite recycling, apoptotic blebs lacking IgG did not translocate p65 to the nucleus, indicating that IgG was responsible for NF-κB activation (Fig. 6 *D* and *E*). To determine whether NF-κB activation in MRL/*lpr* MFs was the consequence of TRIM21, we diminished intracellular TRIM21 levels by using shRNA. Targeting TRIM21 in B6 and MRL/*lpr* bone marrow-derived macrophages (BMMFs) stably reduced TRIM21 levels compared with transduction with a nontargeting control (Fig. 6*F*). In MRL/*lpr* MFs where TRIM21 levels were diminished, phagocytosis of IgG-ICs reduced the nuclear p65 levels 3.4-fold, levels comparable to B6. In contrast, cells transduced with the nontargeting shRNA did not change nuclear p65 levels (Fig. 6 *G* and *H*). Thus, the inability to mature the phagolysosome allows IgG from ICs to leak into the cytosol and activate TRIM21.

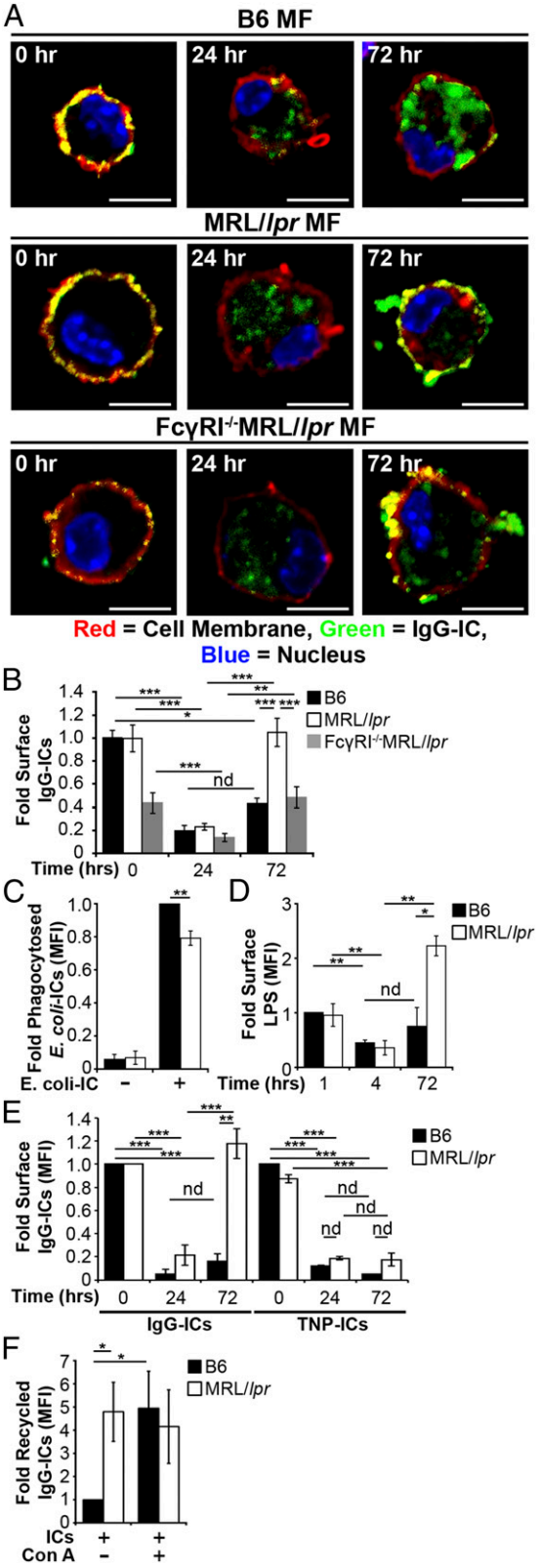

Fig. 4. IgG-ICs recycle and accumulate on the cell membrane of MRL/*lpr* MFs. (*A* and *B*) BMMFs from the indicated mice were cultured with IgG-ICs and examined over time by confocal imaging; four experiments, 3–4 mice, 17–23 cells. A representative image of a MF from the indicated mice (*A*) and quantification of IgG-IC colocalization with the cell membrane for all cells imaged (*B*) is presented. BMMFs were cultured with GFP-expressing *E. coli*-ICs for 1 h. At indicated time points relative levels (to B6+*E. coli*-IC) of phagocytosed *E. coli*-ICs (*C*) and extracellular LPS (relative to B6 1 h; MFI = 6.79–9.32) were quantified by flow cytometry; three experiments, three mice (*D*). BMMFs were cultured with fluorescent IgG-ICs or TNP-ICs for the indicated time. (*E*) Relative levels (to B6 0 h) of surface ICs were quantified by flow cytometry at indicated time points; *Left*, five experiments, five mice; *Right*, two experiments, two mice. (*F*) BMMFs cultured ± concanamycin A (20 ng/mL) were exposed to fluorescently tagged IgG-ICs for 72 h and assessed for relative levels (to B6+ICs-Con A) of recycled IgG-ICs by flow cytometry; 5–6 experiments, 5–6 mice. Error bars = SEM. Student *t* test or ANOVA, nd > 0.05, $*P \leq 0.05$, $**P \leq 0.01$, $***P \leq 0.001$. (Scale bars: 5 μm.)

The activation of TRIM21 by IgG promotes its monoubiquitination, which acts as a docking site for E2 Ube2N/Ube2V2, inducing TRIM polyubiquitination and proteasomal degradation (49, 50). To assess TRIM21 activity in vivo, we quantified the levels of ubiquitinated TRIM21 in ex vivo splenic myeloid cells from B6 and MRL/*lpr* mice. Consistent with TRIM21 activity, we found that splenic myeloid cells from MRL/*lpr* mice had 85-fold more monoubiquitinated TRIM21 compared with ex vivo B6 myeloid cells. Polyubiquitination was not evident (Fig. 6 *I* and *J*). IgG was necessary for TRIM21 ubiquitination because ex vivo myeloid cells from age-matched AID$^{-/-}$MRL/*lpr* mice (lack IgG) had significantly less ubiquitinated TRIM21 (13.5-fold vs. 85-fold) compared with B6 myeloid cells. Acute activation of TRIM21 stabilizes IRF3, whereas chronic activation increases IRF7 levels by activating NF-κB (46, 47). In ex vivo myeloid cells from MRL/*lpr* mice, we found that ubiquitinated TRIM21 was coincident with nuclear translocation of p65 and heightened levels of IRF7 protein, but not with heightened IRF3 (Fig. 6*K*). The finding that IRF7 protein levels are selectively increased suggests that TRIM21 activation in myeloid cells from MRL/*lpr* mice is not an acute event, but instead, induced by chronic activation through IgG.

Impaired Lysosomal Maturation Results in Heightened Intracellular TLR Activation. Diminished lysosomal maturation allows IgG and nuclear antigens to leak into the cytosol and activate innate sensors. However, a large fraction of IgG-ICs remains inside the phagosome and is capable of activating TLRs. Coupled with heightened IRF7 levels from activated TRIM21 (Fig. 6*H*), phagosomal TLR ligands could heighten IFNα secretion through the activation of TLR7 and TLR9 (TLR7/9). To assess whether the prolonged residency of nuclear antigens within the phagolysosome activates intracellular TLRs, we quantified interleukin-1 receptor-associated kinase 1 (IRAK1) levels in MFs 24 h after exposure to IgG-ICs. This time point was sufficient for B6 MFs to degrade the IgG-ICs, but was before recycling of IgG-ICs in MRL/*lpr* MFs (Fig. 4 *A* and *B*). We found that MRL/*lpr* MFs exposed to IgG-ICs showed a 2.8-fold decrease in IRAK1 levels, consistent with TLR activation (Fig. 7*A*). Chloroquine, an acidotropic molecule that binds double- and single-stranded nucleotides and sterically hinders their binding to TLRs (51), restored IRAK1 levels supporting that TLR7/9 are activated in MFs that fail to degrade IgG-ICs. Further, impairing lysosomal acidification with concanamycin A prevented the degradation of IgG-ICs in B6 MFs (Fig. 4*F*) and reduced IRAK1 levels to those found in MRL/*lpr* MFs (Fig. 7*A*). Therefore, the impaired lysosomal acidification in MRL/*lpr* MFs is sufficient to heighten TLR activation in the presence of IgG-ICs.

Formation of the TLR–MyD88–IRAK1 complex downstream of TLR7/9 promotes phosphorylation and nuclear translocation of IRF7, resulting in the production of type 1 IFN (52). To assess whether impaired degradation of IgG-ICs promotes nuclear translocation of IRF7, we cocultured MRL/*lpr* MFs with IgG-ICs and found they exhibited a twofold increase in nuclear IRF7 levels (Fig. 7 *B* and *C*) that was sustained for 24 h. IgG-ICs did not localize all IRF proteins to the nucleus as IRF3 remained cytoplasmic (Fig. 7*C*). Reducing the lysosomal burden through loss of FcγRI also reduced the nuclear translocation of IRF7 in MRL/*lpr* MFs to levels comparable to B6. These findings were not an artifact of BMMFs because ex vivo myeloid cells from MRL/*lpr* mice also showed a twofold increase in nuclear IRF7,

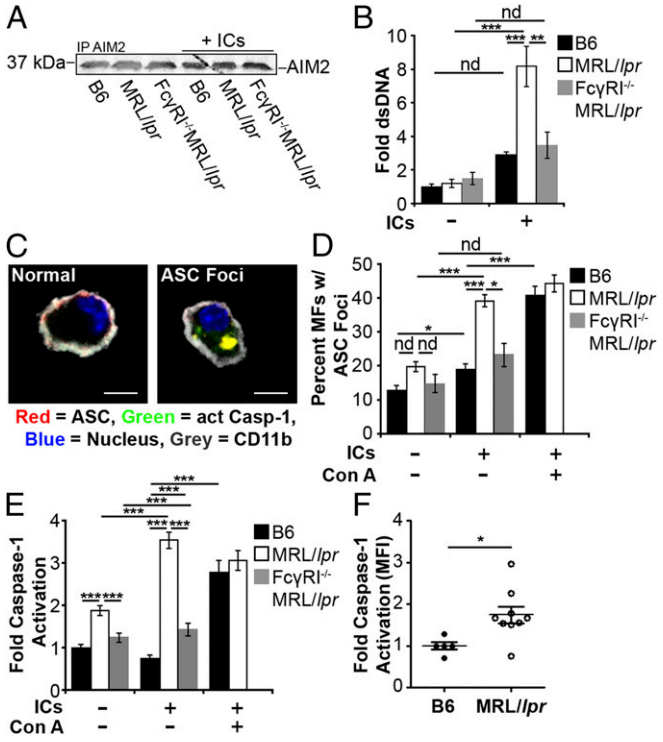

Fig. 5. Impaired lysosomal maturation allows dsDNA to leak into the cytosol and activate AIM2. BMMFs were stimulated for 4 h with Hoechst-labeled IgG-ICs (*A* and *B*). (*A*) A representative blot of immunoprecipitated AIM2 (5–8 × 10^6 cells) is shown. (*B*) Relative levels (to B6 untreated) of fluorescent DNA isolated from the AIM2 immunoprecipitation were quantified by using a fluorescent plate reader; four experiments, four mice. (*C*–*E*) BMMFs were stimulated for 4 h with IgG-ICs ± concanamycin A (20 ng/mL) and then examined for the formation of ASC foci and caspase-1 activation by confocal imaging. A representative image of a MF, with and without ASC foci is presented (*C*). (Scale bars: 5 μm.) The percentage of cells with ASC foci for each experiment (*D*) and relative levels (to B6 untreated) of caspase-1 activation (*E*) was quantified for all cells imaged; 10 experiments, 2–10 mice, 63–364 cells. (*F*) Relative levels (to B6) of caspase-1 activation was measured in splenic myeloid cells ($CD11b^+$) by flow cytometry; four experiments, 5–9 mice (≥17 wk; active disease confirmed with kidney H&E). Error bars = SEM. Student *t* test or ANOVA, nd > 0.05, $*P \leq 0.05$, $**P \leq 0.01$, $***P \leq 0.001$.

whereas nuclear IRF3 was not elevated (Fig. 7*D*). Collectively, the data support a model wherein impaired lysosomal maturation prolongs phagolysosomal residency of IgG-ICs, facilitating chronic intracellular activation of IRAK-coupled TLRs.

The inability to degrade IgG-ICs resulted in increased levels of IRF7 and heightened intracellular TLR activation. Combined, these events could elevate IFNα secretion (52). To assess this possibility, we cultured MRL/*lpr* MFs with IgG-ICs (12, 24 h) and found they secreted two- and threefold more IFNα (Fig. 7*E*). The production of IFNα was a consequence of FcγRI-mediated internalization because IFNα levels secreted by $Fc\gamma RI^{-/-}$MRL/*lpr* MFs were comparable to B6. It was also, in part, a consequence of TLR7 and/or TLR9 because MRL/*lpr* MFs deficient in TLR7 and TLR9 ($TLR7^{-/-}$x$TLR9^{-/-}$/MRL/*lpr*) secreted 3.2-fold less IFNα compared with MRL/*lpr* MFs. The data indicate that FcγRI is required for IFNα secretion by MRL/*lpr* MFs, and that activation of TLR7 and/or TLR9 contributes to ∼70% of the IFNα produced. These findings are consistent with a model wherein diminished lysosomal maturation promotes the accumulation of IgG-ICs in the phagolysosome of MRL/*lpr* MFs activating TLR7 and/or TLR9 and contributing to IFNα secretion.

Discussion

The mechanism underlying the accumulation of IgG-ICs in the periphery of SLE patients has been highly debated. A number of observational studies showed that MFs have intrinsic defects in the phagocytosis of latex beads, apoptotic cells, IgG-ICs, bacteria, and yeast (10, 34, 35, 53). Other studies found that phagocytosis is intact, but the ability to degrade the internalized cargo is impaired (35, 54, 55). We find that lupus-prone MRL/*lpr* MFs phagocytose and traffic IgG-ICs to lysosomal structures, but that the lysosomal structures were unable to mature and acidify. As a result, the IgG-ICs were not degraded and recycled back to the cell membrane. Hematopoietic cells from SLE patients have high levels of IgG and nuclear antigens (32), and they express LAMP1/2 on the cell surface (56). These findings support the idea that the lysosomal compartment has trafficked to the membrane and are consistent with our data showing that MFs from lupus-prone mice accumulated high levels of nuclear antigens (Fig. 1) as a consequence of the recycling of undegraded IgG-ICs from the lysosome (Fig. 4). Interestingly IgG-ICs, apoptotic blebs, and *E. coli*-ICs recycled to the cell membrane, whereas TNP-ICs were degraded, suggesting that the size and/or content of the cargo impairs the lysosome. Alternatively, the opsonin coating the incoming apoptotic debris could impact lysosomal maturation. Combined, these findings could explain the variability of previous studies aimed at identifying defects in SLE monocytes.

Spontaneous SLE has been linked to alterations in expression (57) and activation of TLR7/9 (17, 18), dysregulation of the cytosolic sensors p202 and AIM2 (24, 25), and polymorphisms (21) and heightened expression in TRIM21 (22). We now define that defective degradation of FcγR-bound cargo in the lysosome is a critical upstream event that overburdens the phagolysosome. Prolonged intracellular residency of IgG-ICs promoted the activation of TLRs and the permeabilization of the phagolysosomal membrane, allowing IgG and nuclear antigen to access the cytosol and activate innate sensors. Other enzymes critical in degrading nuclear antigens independent of lysosomes including RNase H2 (58), DNase I (59, 60), and DNase III (TREX1) (61) have been implicated in SLE and may operate in concert with impaired lysosomal maturation to promote autoimmunity. Collectively, our findings identify the events underlying the accumulation of nuclear antigens and activation innate sensors that promote autoantibody, IFNα, and heightened apoptosis in SLE.

Although this study focuses on defining how nuclear antigens accumulate on MFs, it is important to keep in mind that nuclear antigen accumulates on DCs and B and T cells (32). Thus, it is possible that other cells may harbor defects in lysosomal maturation, contributing other disease manifestations. For example, diminished lysosomal maturation in plasmacytoid dendritic cells could heighten secretion of IFNα (19), whereas the same defect in MFs and neutrophils may heighten cell death (62). Further, the presence of nuclear self-antigens on the cell surface could provide a source of high avidity antigen that renews BCR signaling and activates autoreactive B cells (63), facilitates uptake of TLR ligands by BCR-mediated endocytosis (17), and positions autoreactive B cells to further differentiate into memory cells if T-help is available (64). Thus, the same overarching lysosomal defect may contribute to the activation of multiple cell types in SLE.

Overlapping autoimmune diseases are common in patients diagnosed with SLE including diabetes (65), rheumatoid arthritis (66), and Sjögren's syndrome (67). Recent GWAS studies have identified common genetic polymorphisms including the major histocompatibility complex, TNFAIP3, PTPN22 (68), STAT4 (69), and CD40 (70) that span multiple autoimmune diseases, although their functional role in breaking tolerance is unknown. Our finding that punctate IgG accumulates on MFs from multiple murine models of autoimmunity including SLE, diabetes, and rheumatoid arthritis is interesting because it might reflect that aggregated FcγR/IgG-ICs are common to multiple autoimmune diseases. Further, the IgG did not colocalize with high levels of nuclear antigens, suggesting that the antigens contained in the IgG-ICs might be disease-specific, thus activating the immune system in different ways. Therefore, the accumulation of punctate IgG on the surface of MFs from NOD and K/BxN mice raises the possibility that impaired lysosomal maturation underlies other autoimmune diseases.

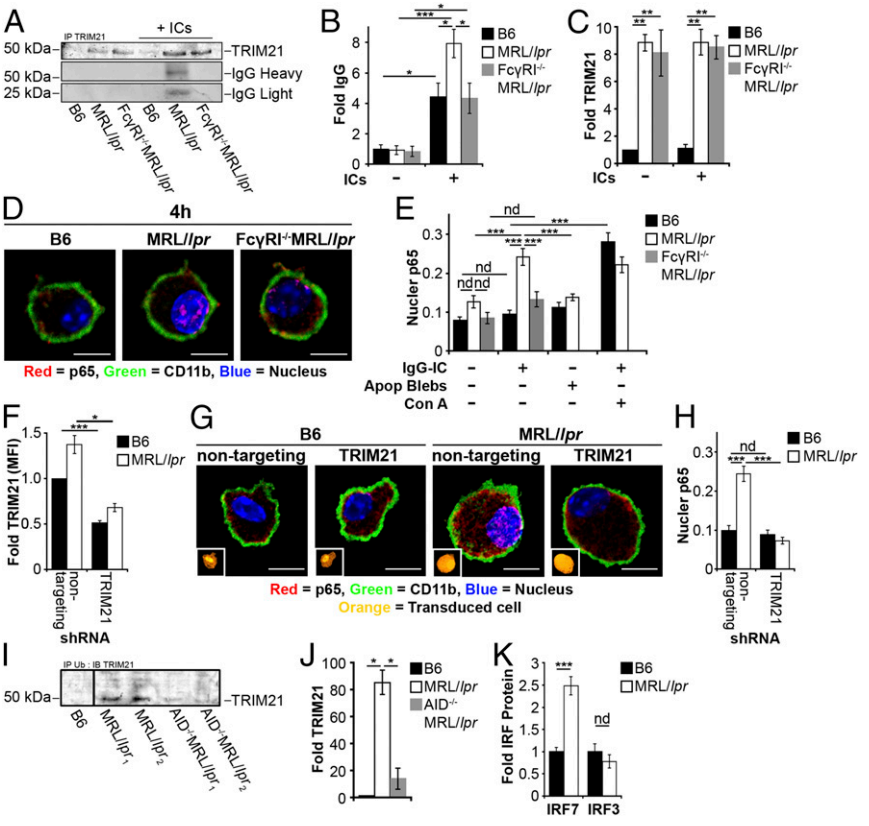

Fig. 6. Impaired lysosomal maturation allows IgG to leak into the cytosol and activate TRIM21. BMMFs were stimulated with fluorescently tagged IgG-ICs (4 h), and TRIM21 was immunoprecipitated (5–8 × 10^6 cells) (*A*–*C*). (*A*) Representative blots of TRIM21 and IgH/IgL chains is shown. (*B*) Relative levels (to B6 untreated) of fluorescent IgG isolated from TRIM21 immunoprecipitates; seven experiments, seven mice. (*C*) Relative levels (to B6 untreated) of immunoprecipitated TRIM21 was quantified by densitometry; three experiments, three mice. (*D* and *E*) Nuclear translocation of p65 subunit of NF-κB was quantified in BMMFs stimulated for 4 h with IgG-ICs or apoptotic debris (lacking IgG), ± concanamycin A (20 ng/mL); six experiments, 3–6 mice, 16–57 cells. Representative image of p65 nuclear localization in MFs from the indicated mice (*D*) and quantification of p65 colocalization with the nucleus of all cells imaged (*E*) is presented. (*F*–*H*) BMMFs were transduced with lentivirus expressing indicated shRNA. Relative levels of TRIM21 (to B6+nontargeting; MFI = 2.57–7.25) in transduced cells (GFP^+) were quantified by flow cytometry; three experiments, three mice (*F*), and nuclear translocation of the p65 subunit of NF-κB was quantified in transduced cells (GFP^+) stimulated for 4 h with IgG-ICs; two experiments, two mice, 20–22 cells (*G* and *H*). Localization of p65 in MFs from the indicated mice (*G*) and quantification of p65 colocalization with the nucleus (*H*) is presented. (*I* and *J*) Ubiquitin was immunoprecipitated from splenic myeloid cells ($CD11b^+$; 35 × 10^6 cells) and immunoblotted for TRIM21; two experiments, 4–5 mice (≥17 wk). A representative blot of TRIM21 following immunoprecipitation of ubiquitin (*I*) and relative levels (to B6) of ubiquitinated TRIM21 was quantified by densitometry (*J*) is presented. Splenic myeloid cells ($CD11b^+$) were analyzed for relative levels (to B6) of IRF7 and IRF3 by confocal microscopy; two experiments, two mice, 10–28 cells (*K*). Error bars = SEM. Student *t* test or ANOVA, nd > 0.05, $*P \leq 0.05$, $**P \leq 0.01$, $***P \leq 0.001$. (Scale bars: 5 μm.)

Materials and Methods

Mice. C57BL/6 (B6) and MRL/MpJ-*Tnfrs6*^{lpr}/J (MRL/*lpr*; JAX mice Stock 000485) colonies were maintained in an accredited animal facility at University of North Carolina at Chapel Hill. Experimental methods were approved by the University of North Carolina's Institutional Animal Care and Use Committee (IACUC). NZM2410 mice (71) were obtained from Gary Gilkeson (mice were 12–22 wk of age; Medical University of South Carolina, Charleston, SC), $AID^{-/-}$MRL/*lpr* mice (72) from Marilyn Diaz, National Institute of Environmental Health Sciences (NIEHS), Research Triangle Park, NC, NOD mice from Roland Tisch (blood glucose levels > 500 mg/dL; University of North Carolina), K/BxN mice (73) from Christophe Benoist (clinical score = 10, ankle thickening = 3.85–3.95 mm; Harvard Medical School, Boston), and C57BL/6-Tg(UBC-GFP)30Scha/J (GFP-expressing) mice (74) from Bill Goldman, University of North Carolina. We generated $Fc\gamma RI^{-/-}$MRL/*lpr* mice by backcrossing $Fc\gamma RI^{-/-}$/C57BL/6 mice to MRL/*lpr* mice for 10 generations. $TLR7^{-/-}$/MRL/*lpr* and $TLR9^{-/-}$/MRL/*lpr* mice were reconstituted from sperm (75) and then intercrossed to generate $TLR7^{-/-}$ × $TLR9^{-/-}$/MRL/*lpr* mice.

Reagents. Antibodies specific for LAMP1 and CD11b were purchased from BD Biosciences; LC3A from Cell Signaling; goat anti-rabbit IgG and rabbit anti-goat IgG from Molecular Probes; AIM2, ASC, TRIM21, p65, IRAK1, IRF3, and IRF7 from Santa Cruz Biotechnologies; anti-IgG from Jackson ImmunoResearch; and anti-LPS (*Escherichia coli* J5) from Thermo Scientific. Concanamycin A and chloroquine diphosphate salt were purchased from Sigma-Aldrich, Immunogold conjugate EM streptavidin from BB International, and $TNP_{20}KLH$ from Biosearch Technologies. Antibodies specific to Smith (Sm; 2.12.3), nucleosome (PL2-3), CD16/32 (2.4G2), and TNP (Hy1.2) were purified from hybridoma culture supernatant by using protein G-Sepharose (GE Healthcare) then left unlabeled or conjugated with Alexa Fluor according to the manufacturer's instructions (Molecular Probes). Fluorescent molecules LysoSensor, dihydrorhodamine 123, and CellMask were purchased from Molecular Probes, and FAM-FLICA caspase-1 assay kit from ImmunoChemistry Technologies. LI-COR blocking buffer, IRDye680-, and IRDy800-conjugated antibodies (anti-rabbit, anti-mouse, anti-goat) were purchased from LI-COR Biosciences. To differentiate BMMFs, we generated L929 cell (European Collection of Cell Cultures) supernatant by plating 2.5 × 10^5 cells into a T150 flask with 50 mL of D10 media [DMEM with 10% (vol/vol) FBS, 1 mM sodium pyruvate, 50 μg/mL gentamicin, 100 μg/mL Pen/Strep, 2 mM L-glutamine, 50 nM βmercaptoethanol (β-ME)]. After 12 d, supernatant was collected and filtered.

Splenocyte Isolation. Spleens from mice were ground between frosted glass slides and filtered through a 70-μm filter to create a single-cell suspension in PBS. Pelleted cells were resuspended in 2 mL of NH_4Cl_2 (0.154 M) for 7 min at room temperature, and then filtered through a 40-μm filter into PBS. Cells were pelleted, then resuspended at 10^8 cells/mL and used for experiments. Alternatively, $CD11b^+$ splenocytes were purified per manufacturer's instructions (Stemcell Technologies).

BMMF Cultures. Single-cell suspensions of bone marrow were prepared from the tibias and femurs of mice. Mononuclear cells were isolated by using Lympholyte Separation Medium (CEDARLANE Laboratories), plated in a 60-mm Petri dish with 6 mL of MF differentiation media [D10 media with 10% (vol/vol) L-cell supernatant], and cultured overnight (37 °C, 5% CO_2). Nonadherent cells were plated into nontissue culture-treated 100-mm Petri dishes (0.75–1 mL cells per Petri dish) with 7 mL of fresh MF differentiation media. To promote MF differentiation, cells were incubated for 6 d (37 °C, 5% CO_2) with an additional 5 mL of MF differentiation media being added on day 4. The resulting BMMFs were removed from the dish by washing with ice cold PBS. BMMF cultures were 98% $CD11b^+$, $I\text{-}A^{lo}$, and $B7.2^{lo}$.

Formation of Immune Complexes.

IgG-ICs. Single-cell suspensions of thymocytes were prepared from 5- to 8-wk mice, irradiated (600 rads), and cultured 16–18 h in 10 mL of PBS (37 °C, 5% CO_2). Apoptotic thymocytes were centrifuged for 5 min (350 × *g*), and the supernatant containing apoptotic debris was incubated with autoantibodies (2.12.3 or PL2-3) on ice for 30 min (6.67 μg of Ab/1 mL of supernatant). IgG-ICs were pelleted (160,000 × *g*) at 4 °C for 45 min and resuspended in 250 μL of R10 media [RPMI with 10% (vol/vol) FBS, 1 mM sodium pyruvate, 50 μg/mL gentamicin, 100 μg/mL Pen/Strep, 2 mM L-glutamine, 50 nM β-ME].

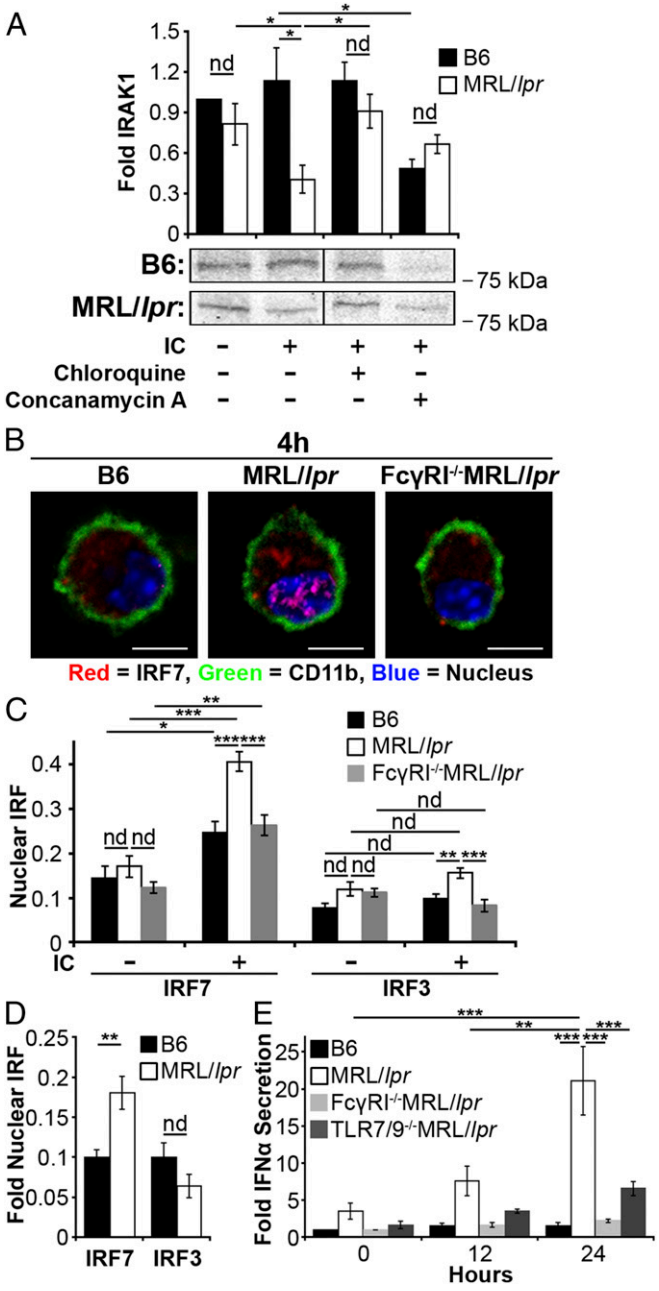

Fig. 7. Impaired lysosomal maturation promotes intracellular TLR activation and IFNα secretion. (*A*) BMMFs (1–1.5 × 10^6 cells) were stimulated for 24 h with IgG-ICs ± hydroxychloroquine (50 μg/mL) or ± concanamycin A (20 ng/mL); five experiments, 3–5 mice. IRAK1 was immunoblotted from whole cell lysates and relative levels (to B6 untreated) of IRAK1 were quantified by densitometry. A representative IRAK1 blot is shown. (*B* and *C*) BMMFs were stimulated with IgG-ICs (4 h), and the nuclear translocation of IRF7 or IRF3 was quantified by confocal microscopy; four experiments, 3–4 mice, 20–42 cells. (Scale bars: 5 μm.) A representative image of a MF from the indicated mice (*B*) and quantification of IRF colocalization with the nucleus of all cells imaged (*C*) is presented. (*D*) Splenic myeloid cells ($CD11b^+$) were analyzed for nuclear IRF7 and IRF3 by confocal microscopy; two experiments, two mice (≥17 wk; active disease confirmed with kidney H&E), 10–28 cells. Supernatants from IgG-IC stimulated BMMFs were collected at the indicated time points and cocultured with WISH cells. Relative levels (to B6 0 h) of IFIT message as an indirect measure of IFNα were quantified by RT-PCR (*E*); three experiments, three mice. Error bars = SEM. Student *t* test or ANOVA, nd > 0.05, $*P \leq 0.05$, $**P \leq 0.01$, $***P \leq 0.001$.

TNP-ICs. TNP_{20}-KLH was incubated with anti-TNP antibody (Hy1.2) on ice for 30 min (30 μg of Ab/1 μg of TNP-KLH). TNP-ICs were pelleted (160,000 × *g*) at 4 °C for 45 min and resuspended in 200 μL of R10 media (as above).

E. coli-ICs. GFP-expressing *E. coli* (76) was incubated with anti-LPS at room temperature for 2 h (1.5 μg/6.25 × 10^6 *E. coli*) in the presence of gentamicin (10 μg/1 mL). *E. coli*-ICs were cultured with BMMFs [multiplicity of infection (MOI) = 25].

Fluorescent Microscopy. All confocal microscopy used a Zeiss 710 confocal microscope with a 63× 1.4 N.A. (oil) PLAN APO lens and Zeiss Zen software. All two-photon microscopy used an Olympus FlouView FV1000MPE multiphoton microscope with a 25× 1.05 N.A. (water) XLPlan N lens and Olympus FluoView software. Cells were randomly selected from many fields of view across the coverslip. Excluded cells were clumped (5–15% of the cells), unhealthy (5–15% of the cells, determined by Hoechst staining), or improperly stained (< 2% of the cells). Data were analyzed by using ImageJ.

IgG-IC/apoptotic bleb localization. BMMFs were cultured in the presence of Alexa488-labeled IgG-ICs or GFP-expressing apoptotic debris in R10 media (as above). After 2 h, the media was aspirated and cells were cultured in fresh R10 media. CellMask and Hoechst 33342 were introduced to BMMFs 15 min before fixation at indicated time points. Cells were fixed in 2% (vol/vol) paraformaldehyde in PBS and transferred to 4 °C for 15 min. Cells were resuspended in FluorSave and loaded onto coverslips for imaging. The membrane localization of IgG-ICs or apoptotic debris was quantified by calculating the Mander's coefficient of colocalization (colocalized pixels/total fluorescent pixels).

Two-photon microscopy/pH quantification. Two hours before imaging, BMMFs were incubated (37 °C, 5% CO_2) on a glass bottom Petri dish (MatTek) in rhodamine-free R10 media (as above). Immediately after adding 40 μL of IgG-ICs and LysoSensor (2 mg/mL), cells were imaged for 1 h. The dye was excited by using two-photon excitation (710 nm), and emissions at 420–460 nm and 495–540 nm were quantified. The ratio of the emission channels were used to determine the pH of the vesicles by using a standard curve generated by exciting LysoSensor with medium of varying pH.

ASC localization/caspase-1 activation. BMMFs were cultured with FAM-FLICA caspase-1 (5 μM) for 20 min before indicated time points. At the indicated time points, cells were washed, fixed with 2% (vol/vol) paraformaldehyde in PBS, and incubated at 4 °C for 15 min. Cells were blocked in 2.4G2 for 30 min at 4 °C in FACS media [2% (vol/vol) FBS, 0.02% NaN_3 in PBS] then stained with an anti-ASC and Hoechst 33342 (1 μg/mL) in permeabilization buffer (PBS with 0.05% Saponin and 0.5% BSA) for 30 min at 4 °C. Cells were washed, stained with goat anti-rabbit IgG-Alexa 647 in permeabilization buffer for 30 min at 4 °C, washed, costained with anti-CD11b in FACS media for 30 min at 4 °C, washed, resuspended in FluorSave, and loaded onto coverslips for imaging. Cells with ASC foci were counted and expressed as a percentage of the total cells. Total caspase-1 activation per cell was quantified (background fluorescence subtracted) and normalized by cell area.

LAMP1/LC3A, IRF, and p65 localization. BMMFs, or splenic myeloid cells ($CD11b^+$) purified by positive selection, were prepared as described for ASC localization/caspase-1 activation except cells were stained for LAMP1 and LC3A, IRF3, IRF7, or p65. The nuclear localization of IRF or p65 was quantified by calculating the Mander's coefficient of colocalization (colocalized pixels/total fluorescent pixels). Total IRF protein in myeloid cells was quantified by determining the total fluorescent pixels (normalized to cell area).

Ex vivo surface stain. Ex vivo splenic cells were fixed in 2% (vol/vol) paraformaldehyde in PBS and incubated for 15 min at 4 °C. Cells were blocked in 2.4G2 for 30 min at 4 °C in FACs media (as above), washed, stained with anti-Sm (2.12.3) and anti-IgG in FACS media for 30 min at 4 °C, washed, stained with anti-CD11b in FACS media for 30 min at 4 °C, and washed. Cells were resuspended in FluorSave and loaded onto coverslips for microscopic imaging. The membrane localization of IgG with Sm was quantified by calculating the Mander's coefficient of colocalization (colocalized pixels/total fluorescent pixels).

Flow Cytometry. All flow cytometry used an 18-color Becton Dickinson LSR II Flow cytometer, and data were acquired by using Becton Dickinson FACSDiva 8.0.1 software.

Recycling of IgG-IC and TNP-IC using flow. BMMFs were incubated (37 °C, 5% CO_2) with 40 μL of Alexa488-labeled IgG-ICs or TNP-ICs in R10 media (as above). To quantify surface-bound ICs at 0 h, phagocytic uptake was impaired by culturing with IgG-ICs on ice for 2 h. This protocol was sufficient to allow the ICs to bind to the surface of the cell but not be phagocytosed. For all other time points, cells were incubated (37 °C, 5% CO_2) for 2 h, then media was replaced to remove all unbound ICs. At indicated time points, cells were blocked in 2.4G2 for 30 min on ice in FACS media (as above), washed, and split into two samples. One sample was incubated with an anti-Alexa488 antibody (quenches Alexa488 fluorescence), whereas the other sample was left in FACS media for

30 min on ice. Both samples were washed and fixed with 2% paraformaldehyde and incubated at 4 °C for 15 min. Surface-bound IgG-ICs were calculated by subtracting the mean fluorescence intensity (MFI) of the quenched sample (intracellular IgG-ICs) from the MFI of the unquenched sample (total IgG-ICs). Values were normalized to B6 0 h.

***E. coli*-IC recycling flow.** BMMFs were incubated (37 °C, 5% CO_2) with *E. coli*-ICs (MOI = 25) in R10 media (as above). Cells were incubated (37 °C, 5% CO_2) for 1 h, then media was replaced to remove all unbound ICs. At indicated time points, cells were blocked in 2.4G2 for 30 min on ice in FACS media (as above), washed, and incubated with Alexa647-labeled anti-LPS in FACS media for 30 min on ice. Samples were washed and fixed with 2% paraformaldehyde, and then incubated at 4 °C for 15 min. Cells were resuspended in FACS media, and the levels of phagocytosed *E. coli*-ICs and surface LPS were quantified by flow cytometry. MFI values for phagocytosed *E. coli*-ICs were normalized to B6+*E. coli*-ICs. MFI for surface LPS was normalized to an isotype control.

Ratiometric flow cytometry. BMMFs were incubated (37 °C, 5% CO_2) for 2 h before the addition of 40 μL of IgG-ICs in R10 media (as above). To quantify a cell that has not acidified, concanamycin A (20 ng/mL) was introduced to one sample from each cell type 2 h before addition of IgG-ICs and left on the cells throughout the experiment. IgG-ICs and LysoSensor (2 mg/mL) were introduced for 30 min, aspirated, and replaced with fresh rhodamine-free R10 media. Cells were incubated until indicated time points and analyzed by flow cytomualifiedetry. The dye was excited with a UV laser (355 nm). Relative pH was quantified by ratioing the MFIs from the emission channels (450/20 nm, 585/42 nm) (normalized to concanamycin A control).

Ex vivo surface stain. Ex vivo splenic cells were prepared as described for "Ex vivo surface stain" in the "Fluorescent Microscopy" section. Cells were resuspended in FACS media, and the MFI of the surface Sm and IgG were determined by flow cytometry and normalized to an isotype control.

Ex vivo caspase-1 activation. Ex vivo splenic cells were cultured with FAM-FLICA caspase-1 (5 μM) for 20 min before fixation. Cells were fixed in 2% paraformaldehyde and incubated for 15 min at 4 °C. Cells were washed, stained with anti-CD11b in FACS media for 30 min at 4 °C, and washed. Cells were resuspended in FACS media, and the MFI of the surface Sm was determined by flow cytometry and normalized to an isotype control. Values are normalized to B6.

TRIM21 flow cytometry. Following viral transduction, BMMFs were fixed with 2% (vol/vol) paraformaldehyde in PBS, then incubated at 4 °C for 15 min. Cells were blocked in 2.4G2 for 30 min at 4 °C in FACS media (as above), washed, and stained with anti-TRIM21 in permeabilization buffer (as above) for 30 min at 4 °C. Cells were washed, stained with rabbit anti-goat IgG-Alexa 647 in permeabilization buffer for 30 min at 4 °C, washed, and resuspended in FACS media. The MFI of the TRIM21 were determined by flow cytometry and normalized to an isotype control.

Cryo-Electron Microscopy. BMMFs were incubated with 40 μL of gold-labeled IgG-ICs for 2 h (37 °C, 5% CO_2). Suspensions of MFs were loaded into gold planchettes (model 16706897; well size 1.2 mm × 200 μm), placed in high pressure-freeze (HPF) holders, and torqued to make a tight seal. Each sample was placed in a HPF chamber where the pressure was increased with cyclohexane to ∼2,000 bars just milliseconds before a blast of liquid nitrogen cooled the assembly at approximately 18,000 °C/sec by using a Leica EM PACT HPF. The pressure and cooling curves were recorded and examined after each run to ensure consistency. Frozen samples were transferred to liquid nitrogen for storage. Samples were then transferred to vials containing 2% osmium tetroxide in dry acetone cooled in liquid nitrogen. The vials were transferred cold to a chamber at −90 °C in a Leica EM AFS freeze substitution device, where samples remained for 72 h. Samples were warmed automatically by using a program that increased the temperature to −20 °C at 4 °C/h, held at −20 °C for 10 h, then warmed at 4 °C/h to 20 °C. The warmed fixed samples were processed for transmission electron microscopy (TEM) by washing with fresh acetone and replacing the acetone with propylene oxide, embedding in epon (EMS EMbed-812), and hardening at 60 °C. Thin sections, 60–70 nm thick, were cut with a diamond knife on a Leica Ultracut UTC and stained with uranyl acetate and lead citrate. Stained thin sections were examined with an FEI Tecnai T12 G2 TEM at 80 kV by using a Gatan 794 digital camera and Gatan Digital Montage software to prepare up to 5 × 5 montages of selected MFs imaged at 6,000–30,000×.

Immunoprecipitation and Western Blot. Lysates were prepared by the addition of lysis buffer containing 1% CHAPS, 150 mM NaCl, 10 mM Tris (pH 7.5), 2 mM sodium orthovanadate, 1 mM PMSF, 0.4 mM EDTA, 10 mM NaF, and 1 μg/mL each of aprotinin, leupeptin, and α1-antitrypsin (in water) to cell pellets. Lysates were held on ice for 10 min followed by the removal of particulate material by centrifugation at 12,000 × *g* for 10 min at 4 °C.

Antibodies used in the immunoprecipitations were conjugated to cyanogen bromide-activated Sepharose 4B according to manufacturer's instructions (Amersham Pharmacia Biotech). Approximately 2 μg of precipitating antibodies was incubated with 1.5×10^6 cell equivalents of cleared lysate for 1 h at 4 °C. Immunoprecipitates were washed twice with lysis buffer, resuspended in reducing SDS/PAGE sample buffer, and fractionated by 10% SDS/PAGE. Separated proteins were transferred to Immobilon-FL membranes. Membranes were blocked in LI-COR Blocking Buffer, incubated with the various immunoblotting Abs followed by the appropriate fluorophore-conjugated secondary Abs. Immunoreactive proteins were detected by using a LI-COR Odyssey infrared imaging system with Odyssey 3.0 software.

Plate Reader. All analysis used a Tecan M200 fluorescence plate reader.

ROS assay. BMMFs were incubated (37 °C, 5% CO_2) for 2 h before the addition of 40 μL of IgG-ICs in R10 media (as above) in an opaque 96-well plate. Thirty minutes before indicated time points, dihydrorhodamine 123 (3 μg/mL) was added to each well. At the indicated time points, cells were washed, fixed with 2% paraformaldehyde, and transferred to 4 °C for 15 min. Wells were analyzed in FACS media (as above). Each sample had an *N*-acetylcysteine–treated control (1 mM). Fluorescent readings were normalized to *N*-acetylcysteine–treated B6 MFs.

Immunoprecipitation assay. All beads from immunoprecipitation sample were added to a single well in an opaque 96-well plate in PBS. Wells were analyzed for Hoechst-labeled dsDNA (AIM2 immunoprecipitation) and Alexa647-labeled IgG (TRIM21 immunoprecipitation). All fluorescent readings were normalized to the background fluorescence of beads alone.

BMMF Transduction. BMMFs were prepared as described above. On day 3, cells in a 24-well low cluster plate were transduced with lentiviral particles (SMARTvector Lentiviral mouse TRIM21 mCMV-TurboGFP shRNA; MOI = 40; polybrene = 5 μg/mL) according to manufacturer's instructions (Dharmacon). Separate cells were transduced with SMARTvector Nontargeting mCMV-TurboGFP control particles. On days 5 and 6, culture medium was replenished with an additional 750 μL of macrophage differentiation media. Stably transduced cells expressed GFP by day 6 (8–20% of the culture).

WISH Cell IFNα Assay. WISH cells (product no. CCL-25; American Type Culture Collection) were grown in minimum essential medium supplemented with L-glutamine (2 mM), Hepes (20 mM), penicillin (100 units/mL), streptomycin (100 μg/mL), and 10% (vol/vol) FBS (37 °C, 5% CO_2). To measure IFNα levels, we quantified mRNA of IFN-regulated genes as described (77). WISH cells were plated (0.5×10^5 cells per 0.1 mL) in 96-well flat bottom plates and cultured with media alone, recombinant mouse IFNα (100 units/mL; BioSource International), or BMMF supernatant (200 μL) for 24 h (37 °C, 5% CO_2). WISH cells were lysed, RNA extracted (RNeasy Mini Kit; Qiagen), and cDNA prepared from 500 ng of RNA (iScript c-DNA Synthesis Kit; Bio-Rad Laboratories). The cDNA obtained from each sample was diluted 1:60, and 2 μL was amplified in a 20-μL real-time quantitative PCR by using 10 mM forward and reverse primers and the 2× iQ SYBR Green Supermix (Roche Laboratories).

Statistics. Error bars represent the SEM. For the TIRF assay, error bars represent the variation between individual IgG-ICs on the surface of the cell. For other microscopy-based experiments, the error bars represent the variation between cells. In all other assays, the error bars represent the variation between mice. All *P* values were calculated by using an unpaired *t* test (two groups) or an ANOVA (groups ≥ 3). Significance is indicated on the graphs ("nd" $P > 0.05$, $*P \leq 0.05$, $**P \leq 0.01$, $***P \leq 0.001$).

ACKNOWLEDGMENTS. We thank Drs. Roland Tisch and Nick Spidale for NOD mice, Dr. Gary Gilkeson for NZM2410 mice, Dr. Christophe Benoist for K/BxN mice, Drs. Edward Miao and Bill Goldman for the GFP-*E. coli* and B6/GFP mice, Flow Cytometry Core (NIH Grant NCI P30CA016086), the Microscopy Services Laboratory (NIH Grant CA 16086-26) for their support, and Robert Currin at the University of North Carolina Olympus Center for assistance with two-photon imaging. This work was supported by NIH Grants R01AI070984, R21AI105613, and R21AR064951 and a grant from the Alliance for Lupus Research. A.J.M. was supported by NIH Grant 5T32AI07273.

1. Elkon K, Casali P (2008) Nature and functions of autoantibodies. *Nat Clin Pract Rheumatol* 4(9):491–498.
2. Poon IK, Lucas CD, Rossi AG, Ravichandran KS (2014) Apoptotic cell clearance: Basic biology and therapeutic potential. *Nat Rev Immunol* 14(3):166–180.
3. Hepburn AL, et al. (2007) In vivo evidence for apoptosis in the bone marrow in systemic lupus erythematosus. *Ann Rheum Dis* 66(8):1106–1109.
4. Klemperer P (1948) The pathogenesis of lupus erythematosus and allied conditions. *Ann Intern Med* 28(1):1–11.

5. Kuhn A, et al. (2006) Accumulation of apoptotic cells in the epidermis of patients with cutaneous lupus erythematosus after ultraviolet irradiation. *Arthritis Rheum* 54(3):939–950.
6. Bardana EJ, Jr, Harbeck RJ, Hoffman AA, Pirofsky B, Carr RI (1975) The prognostic and therapeutic implications of DNA:anti-DNA immune complexes in systemic lupus erythematosus (SLE). *Am J Med* 59(4):515–522.
7. Botto M, et al. (1998) Homozygous C1q deficiency causes glomerulonephritis associated with multiple apoptotic bodies. *Nat Genet* 19(1):56–59.
8. Hanayama R, et al. (2004) Autoimmune disease and impaired uptake of apoptotic cells in MFG-E8-deficient mice. *Science* 304(5674):1147–1150.
9. Ballantine L, et al. (2015) Increased soluble phagocytic receptors sMer, sTyro3 and sAxl and reduced phagocytosis in juvenile-onset systemic lupus erythematosus. *Pediatr Rheumatol Online J* 13:10.
10. Fries LF, Mullins WW, Cho KR, Plotz PH, Frank MM (1984) Monocyte receptors for the Fc portion of IgG are increased in systemic lupus erythematosus. *J Immunol* 132(2):695–700.
11. Hu CY, et al. (2009) Genetic polymorphism in milk fat globule-EGF factor 8 (MFG-E8) is associated with systemic lupus erythematosus in human. *Lupus* 18(8):676–681.
12. Li Y, et al. (2009) Increased expression of FcgammaRI/CD64 on circulating monocytes parallels ongoing inflammation and nephritis in lupus. *Arthritis Res Ther* 11(1):R6.
13. Pickering MC, Botto M, Taylor PR, Lachmann PJ, Walport MJ (2000) Systemic lupus erythematosus, complement deficiency, and apoptosis. *Adv Immunol* 76:227–324.
14. Yamaguchi H, et al. (2010) Aberrant splicing of the milk fat globule-EGF factor 8 (MFG-E8) gene in human systemic lupus erythematosus. *Eur J Immunol* 40(6):1778–1785.
15. Licht R, Jacobs CW, Tax WJ, Berden JH (2001) No constitutive defect in phagocytosis of apoptotic cells by resident peritoneal macrophages from pre-morbid lupus mice. *Lupus* 10(2):102–107.
16. Tas SW, Quartier P, Botto M, Fossati-Jimack L (2006) Macrophages from patients with SLE and rheumatoid arthritis have defective adhesion in vitro, while only SLE macrophages have impaired uptake of apoptotic cells. *Ann Rheum Dis* 65(2):216–221.
17. Lau CM, et al. (2005) RNA-associated autoantigens activate B cells by combined B cell antigen receptor/Toll-like receptor 7 engagement. *J Exp Med* 202(9):1171–1177.
18. Viglianti GA, et al. (2003) Activation of autoreactive B cells by CpG dsDNA. *Immunity* 19(6):837–847.
19. Rönnblom L, Pascual V (2008) The innate immune system in SLE: Type I interferons and dendritic cells. *Lupus* 17(5):394–399.
20. Boulé MW, et al. (2004) Toll-like receptor 9-dependent and -independent dendritic cell activation by chromatin-immunoglobulin G complexes. *J Exp Med* 199(12):1631–1640.
21. Frank MB, et al. (1993) The mapping of the human 52-kD Ro/SSA autoantigen gene to human chromosome 11, and its polymorphisms. *Am J Hum Genet* 52(1):183–191.
22. Oke V, et al. (2009) High Ro52 expression in spontaneous and UV-induced cutaneous inflammation. *J Invest Dermatol* 129(8):2000–2010.
23. Lyons PA, et al. (2010) Novel expression signatures identified by transcriptional analysis of separated leucocyte subsets in systemic lupus erythematosus and vasculitis. *Ann Rheum Dis* 69(6):1208–1213.
24. Roberts TL, et al. (2009) HIN-200 proteins regulate caspase activation in response to foreign cytoplasmic DNA. *Science* 323(5917):1057–1060.
25. Rozzo SJ, et al. (2001) Evidence for an interferon-inducible gene, Ifi202, in the susceptibility to systemic lupus. *Immunity* 15(3):435–443.
26. Lech M, et al. (2015) NLRP3 and ASC suppress lupus-like autoimmunity by driving the immunosuppressive effects of TGF-β receptor signalling. *Ann Rheum Dis* 74(12):2224–2235.
27. Yang Q, et al. (2014) Deregulated NLRP3 and NLRP1 inflammasomes and their correlations with disease activity in systemic lupus erythematosus. *J Rheumatol* 41(3): 444–452.
28. Klarquist J, et al. (2014) STING-mediated DNA sensing promotes antitumor and autoimmune responses to dying cells. *J Immunol* 193(12):6124–6134.
29. Sharma S, et al. (2015) Suppression of systemic autoimmunity by the innate immune adaptor STING. *Proc Natl Acad Sci USA* 112(7):E710–E717.
30. O'Brien BA, Fieldus WE, Field CJ, Finegood DT (2002) Clearance of apoptotic beta-cells is reduced in neonatal autoimmune diabetes-prone rats. *Cell Death Differ* 9(4):457–464.
31. Nakajima T, et al. (1995) Apoptosis and functional Fas antigen in rheumatoid arthritis synoviocytes. *Arthritis Rheum* 38(4):485–491.
32. Kang SA, et al. (2016) Apoptotic debris accumulates on hematopoietic cells and promotes disease in murine and human SLE. *J Immunol*, in press.
33. Bijl M, Reefman E, Horst G, Limburg PC, Kallenberg CG (2006) Reduced uptake of apoptotic cells by macrophages in systemic lupus erythematosus: Correlates with decreased serum levels of complement. *Ann Rheum Dis* 65(1):57–63.
34. Herrmann M, et al. (1998) Impaired phagocytosis of apoptotic cell material by monocyte-derived macrophages from patients with systemic lupus erythematosus. *Arthritis Rheum* 41(7):1241–1250.
35. Kavai M, Szegedi G (2007) Immune complex clearance by monocytes and macrophages in systemic lupus erythematosus. *Autoimmun Rev* 6(7):497–502.
36. Reefman E, et al. (2007) Opsonization of late apoptotic cells by systemic lupus erythematosus autoantibodies inhibits their uptake via an Fcgamma receptor-dependent mechanism. *Arthritis Rheum* 56(10):3399–3411.
37. Bonnerot C, et al. (1998) syk protein tyrosine kinase regulates Fc receptor gamma-chain-mediated transport to lysosomes. *EMBO J* 17(16):4606–4616.
38. Rybicka JM, Balce DR, Khan MF, Krohn RM, Yates RM (2010) NADPH oxidase activity controls phagosomal proteolysis in macrophages through modulation of the lumenal redox environment of phagosomes. *Proc Natl Acad Sci USA* 107(23):10496–10501.
39. Fischbach M (1984) Defective T cell response to presented antigen in autoimmune mice. *J Immunol* 133(5):2365–2368.
40. Yan J, Harvey BP, Gee RJ, Shlomchik MJ, Mamula MJ (2006) B cells drive early T cell autoimmunity in vivo prior to dendritic cell-mediated autoantigen presentation. *J Immunol* 177(7):4481–4487.
41. Kirisits A, Pils D, Krainer M (2007) Epidermal growth factor receptor degradation: An alternative view of oncogenic pathways. *Int J Biochem Cell Biol* 39(12):2173–2182.
42. Sharma M, et al. (2004) Misfolding diverts CFTR from recycling to degradation: Quality control at early endosomes. *J Cell Biol* 164(6):923–933.
43. Manzanillo PS, Shiloh MU, Portnoy DA, Cox JS (2012) Mycobacterium tuberculosis activates the DNA-dependent cytosolic surveillance pathway within macrophages. *Cell Host Microbe* 11(5):469–480.
44. Perrin AJ, Jiang X, Birmingham CL, So NS, Brumell JH (2004) Recognition of bacteria in the cytosol of Mammalian cells by the ubiquitin system. *Curr Biol* 14(9):806–811.
45. Rhodes DA, Trowsdale J (2007) TRIM21 is a trimeric protein that binds IgG Fc via the B30.2 domain. *Mol Immunol* 44(9):2406–2414.
46. McEwan WA, et al. (2013) Intracellular antibody-bound pathogens stimulate immune signaling via the Fc receptor TRIM21. *Nat Immunol* 14(4):327–336.
47. Yang K, et al. (2009) TRIM21 is essential to sustain IFN regulatory factor 3 activation during antiviral response. *J Immunol* 182(6):3782–3792.
48. Marnell L, Mold C, Du Clos TW (2005) C-reactive protein: Ligands, receptors and role in inflammation. *Clin Immunol* 117(2):104–111.
49. Fletcher AJ, Mallery DL, Watkinson RE, Dickson CF, James LC (2015) Sequential ubiquitination and deubiquitination enzymes synchronize the dual sensor and effector functions of TRIM21. *Proc Natl Acad Sci USA* 112(32):10014–10019.
50. Mallery DL, et al. (2010) Antibodies mediate intracellular immunity through tripartite motif-containing 21 (TRIM21). *Proc Natl Acad Sci USA* 107(46):19985–19990.
51. Kuznik A, et al. (2011) Mechanism of endosomal TLR inhibition by antimalarial drugs and imidazoquinolines. *J Immunol* 186(8):4794–4804.
52. Kawai T, et al. (2004) Interferon-alpha induction through Toll-like receptors involves a direct interaction of IRF7 with MyD88 and TRAF6. *Nat Immunol* 5(10):1061–1068.
53. Wu SA, et al. (2013) Impaired phagocytosis and susceptibility to infection in pediatric-onset systemic lupus erythematosus. *Lupus* 22(3):279–288.
54. Kávai M, Csipö I, Sonkoly I, Csongor J, Szegedi GY (1986) Defective immune complex degradation by monocytes in patients with systemic lupus erythematosus. *Scand J Immunol* 24(5):527–532.
55. Matul'skaia LI, Klimov VIu, Riazantseva TA, Pleskovskaia GN (1986) [DNAse II from phagocytes in the study of the pathogenesis of systemic lupus erythematosus]. *Vopr Med Khim* 32(1):32–34.
56. Holcombe RF, et al. (1994) Correlation of serum interleukin-8 and cell surface lysosome-associated membrane protein expression with clinical disease activity in systemic lupus erythematosus. *Lupus* 3(2):97–102.
57. Deane JA, et al. (2007) Control of toll-like receptor 7 expression is essential to restrict autoimmunity and dendritic cell proliferation. *Immunity* 27(5):801–810.
58. Günther C, et al. (2015) Defective removal of ribonucleotides from DNA promotes systemic autoimmunity. *J Clin Invest* 125(1):413–424.
59. Napirei M, et al. (2000) Features of systemic lupus erythematosus in Dnase1-deficient mice. *Nat Genet* 25(2):177–181.
60. Skiljevic D, et al. (2013) Serum DNase I activity in systemic lupus erythematosus: Correlation with immunoserological markers, the disease activity and organ involvement. *Clin Chem Lab Med* 51(5):1083–1091.
61. Lee-Kirsch MA, et al. (2007) Mutations in the gene encoding the 3′-5′ DNA exonuclease TREX1 are associated with systemic lupus erythematosus. *Nat Genet* 39(9):1065–1067.
62. Ren Y, et al. (2003) Increased apoptotic neutrophils and macrophages and impaired macrophage phagocytic clearance of apoptotic neutrophils in systemic lupus erythematosus. *Arthritis Rheum* 48(10):2888–2897.
63. Cambier JC, Gauld SB, Merrell KT, Vilen BJ (2007) B-cell anergy: From transgenic models to naturally occurring anergic B cells? *Nat Rev Immunol* 7(8):633–643.
64. Anderson SM, Tomayko MM, Shlomchik MJ (2006) Intrinsic properties of human and murine memory B cells. *Immunol Rev* 211:280–294.
65. Bruce IN, Urowitz MB, Gladman DD, Ibañez D, Steiner G (2003) Risk factors for coronary heart disease in women with systemic lupus erythematosus: The Toronto Risk Factor Study. *Arthritis Rheum* 48(11):3159–3167.
66. Iaccarino L, et al. (2013) Overlap connective tissue disease syndromes. *Autoimmun Rev* 12(3):363–373.
67. Lockshin MD, Levine AB, Erkan D (2015) Patients with overlap autoimmune disease differ from those with 'pure' disease. *Lupus Sci Med* 2(1):e000084.
68. Cho JH, Feldman M (2015) Heterogeneity of autoimmune diseases: Pathophysiologic insights from genetics and implications for new therapies. *Nat Med* 21(7):730–738.
69. Remmers EF, et al. (2007) STAT4 and the risk of rheumatoid arthritis and systemic lupus erythematosus. *N Engl J Med* 357(10):977–986.
70. Ramos PS, et al.; International Consortium on the Genetics of Systemic Erythematosus (2011) A comprehensive analysis of shared loci between systemic lupus erythematosus (SLE) and sixteen autoimmune diseases reveals limited genetic overlap. *PLoS Genet* 7(12):e1002406.
71. Rudofsky UH, Evans BD, Balaban SL, Mottironi VD, Gabrielsen AE (1993) Differences in expression of lupus nephritis in New Zealand mixed H-2z homozygous inbred strains of mice derived from New Zealand black and New Zealand white mice. Origins and initial characterization. *Lab Invest* 68(4):419–426.
72. Jiang C, et al. (2007) Abrogation of lupus nephritis in activation-induced deaminase-deficient MRL/lpr mice. *J Immunol* 178(11):7422–7431.
73. Kouskoff V, et al. (1996) Organ-specific disease provoked by systemic autoimmunity. *Cell* 87(5):811–822.
74. Schaefer BC, Schaefer ML, Kappler JW, Marrack P, Kedl RM (2001) Observation of antigen-dependent CD8+ T-cell/dendritic cell interactions in vivo. *Cell Immunol* 214(2):110–122.
75. Christensen SR, et al. (2006) Toll-like receptor 7 and TLR9 dictate autoantibody specificity and have opposing inflammatory and regulatory roles in a murine model of lupus. *Immunity* 25(3):417–428.
76. Valdivia RH, Falkow S (1997) Fluorescence-based isolation of bacterial genes expressed within host cells. *Science* 277(5334):2007–2011.
77. Hua J, Kirou K, Lee C, Crow MK (2006) Functional assay of type I interferon in systemic lupus erythematosus plasma and association with anti-RNA binding protein autoantibodies. *Arthritis Rheum* 54(6):1906–1916.